Impedance-Based Monitoring of Ongoing Cardiomyocyte Death Induced by Tumor Necrosis Factor-α

Yiling Qiu,[†] Ronglih Liao,[‡] and Xin Zhang[†]*

[†]Laboratory for Microsystems Technology, Department of Mechanical Engineering, Boston University; and [‡]Brigham and Women's Hospital, Harvard Medical School, Boston, Massachusetts

ABSTRACT   Deregulated cardiomyocyte death is a critical risk factor in a variety of cardiovascular diseases. Although various assays have been developed to detect cell responses during cell death, the capability of monitoring cell detachment will enhance the understanding of death processes by providing instant information at its early phase. In this work, we developed an impedance-sensing assay for real-time monitoring of cardiomyocyte death induced by tumor necrosis factor-α based on recording the change in cardiomyocyte adhesion to extracellular matrix. Electrochemical impedance spectroscopy was employed in impedance data processing, followed by calibration with the electrical cell-substrate impedance-sensing technique. The adhesion profile of cardiomyocytes undergoing cell death processes was recorded as the time course of equivalent cell-substrate distance. The cell detachment was detected with our assay and proved related to cell death in the following experiments, indicating its advantage against the conventional assays, such as Trypan blue exclusion. An optimal concentration of tumor necrosis factor-α (20 ng/mL) was determined to induce cardiomyocyte apoptosis rather than the combinative cell death of necrosis and apoptosis by comparing the concentration-related adhesion profiles. The cardiomyocytes undergoing apoptosis experienced an increase of cell-substrate distance from 59.1 to 89.2 nm within 24 h. The early change of cell adhesion was proved related to cardiomyocyte apoptosis in the following TUNEL test at $t = 24$ h, which suggested the possibility of early and noninvasive detection of cardiomyocyte apoptosis.

INTRODUCTION

Cardiomyocyte loss by cell death is significantly dangerous because it causes irreversible damage to adult hearts because of their very limited regeneration capability. It was reported in a recent publication that cell death, whether by apoptosis or necrosis, can lead to heart failure (1). Currently, in the in vitro study of cardiomyocyte cell death, the most common assays for cell viability are microscopic examination of chemically stained cells. Despite great advances that have been made with these approaches, additional research has been conducted to develop noninvasive techniques for real-time monitoring of cell death. In both necrotic and apoptotic cell death processes, it is a common phenomenon that cells detach from the extracellular matrix (ECM). Especially, cell detachment occurs at the early phase of cell death, which suggests the possibility of detecting ongoing cell death processes by monitoring cell adhesion.

It has long been recognized that electric cell-substrate impedance sensing (ECIS) is a noninvasive and sensitive detecting technique for cell adhesion (2,3). In the last two decades, ECIS sensing has been employed to monitor many types of cells, including fibroblasts, endothelial cells, and cancer cells (4–11). More recently, ECIS research has turned to excitable cells, such as skeletal muscle cells (12) and cardiomyocytes (13,14). Generally, time courses of overall impedance during the biological processes were recorded in time intervals and attributed to various cell behaviors. To extract direct and detailed information from the overall signals, researchers (15,16) further developed advanced data-processing techniques. In these methods, paracellular current flow in the medium gap between cells and electrodes is described in the infinite element model (15,17) where the cell body is assumed to exhibit known and stable capacitance. It has been reported that this advanced ECIS method is capable of detecting vertical motion on the order of 1 nm (3). Combined with other biophysical and biochemical assays, advanced ECIS has been applied to study apoptosis of endothelial cells (18).

However, unlike endothelial cells or fibroblasts in the reported ECIS studies that exhibit known and constant electrical properties because of reliable commercialized cell lines, cardiomyocytes are primarily cultured, which means electrical properties of cardiomyocytes needed in the ECIS calculation are unknown and unstable. This is essentially the bottleneck of ECIS application to cardiomyocyte research. In our previous work (19), impedance spectra obtained in cyclic frequency scanning were used to determine the unknown membrane capacitance of cardiomyocytes based on electrochemical impedance spectroscopy (EIS). A methodology was established on the basis of ECIS and EIS to calculate the equivalent cell-substrate distance, which mader it possible to carry out real-time monitoring of ongoing biological processes in cardiomyocytes and other primary cells.

In this work, the ongoing cardiomyocyte cell death induced by tumor necrosis factor-α (TNF-α) was real-time monitored and recorded in time courses of equivalent

cell-substrate distance calculated by our methodology. Cell adhesion profiles were recorded at multiple TNF-α concentration levels, and the results were compared with those of TBE tests. The comparison showed that our assays picked up cell detachment in advance of obvious difference seen in Trypan blue exclusion (TBE) tests. Furthermore, the distinct cell adhesion profiles indicated that different cell death mechanisms were experienced at different concentration levels. Namely, apoptosis could be the main death mechanism in cardiomyocytes treated with 20 ng/mL TNF-α. Its slowly detaching profile was proven related to cardiomyocyte apoptosis in the following terminal uridine deoxynucleotidyl transferase dUTP nick-end labeling (TUNEL) test.

EXPERIMENTAL SECTION

Fabrication

The fabrication of the biosensing chips was conducted in a microfabrication laboratory. A glass slide was chosen as the substrate material because it could minimize the substrate capacitance and decrease the measurement noise. The electrode voids of the chips were patterned on the slides with photoresist Shipley 1813 in photolithography on the MA6 aligner. Effective adhesion of the metal electrodes to the glass substrate was required; therefore, a chromium layer (125 Å) was first deposited by thermal evaporation, followed by the deposition of the major electrode components with gold (375 Å) (Kurt J. Lesker , Pittsburgh, PA). The metal electrodes were defined in a lift-off process. SiO_2 and SiN_x (Kurt J. Lesker Co.) were deposited with magnetic sputtering to form an insulating layer with a thickness of 1200 Å. Windows were defined in the insulating layer using photolithography and opened by reactive ion etching to access the gold electrode surface. A biosensing chip consisted of 16 circular working electrodes (0.502 mm^2) and one common rectangular counterelectrode (2.0 cm^2). Fig. 1 a shows the configuration of the biosensing chip.

Testing systems

The schematic diagram and photo of our impedance-sensing system is depicted in Fig. 1 b. The biosensing chip was maintained in the incubator at 5% CO_2 and 37°C throughout the electrical measurement to avoid any fluctuations in the testing environment. Inside the incubator, the biosensing chip was mounted to a homemade silicone chamber designed for cell culture. The electrode pads were connected to micromanipulators, which transferred signals through an Agilent 16048A BNC test fixture to the outside of the chamber. The impedance of the electrodes in the chip was measured with an Agilent 4284A LCR meter (Agilent Technologies, Santa Clara, CA). For automatic measurement and data logging, the LCR meter was connected to a computer through a GPIB interface. The impedance measurement process was controlled by LabView (National Instruments Corp., Austin, TX) virtual instruments.

Cardiomyocyte isolation and culture

Left ventricular myocytes were isolated from male Wistar rats according to a previously established protocol with some modifications (20). The rat heart was separated and perfused with Ca^{2+}-free Krebs buffer (0.12 M NaCl, 4.7 mM KCl, 1.2 mM KH_2PO_4, 1.2 mM $MgSO_4$, 25 M $NaHCO_3$, and 12 mM glucose) and enzyme buffer (375 mg/L collagenase and 425 mg/L hyaluronidase in Ca^{2+}-free Krebs buffer). The rat heart was then cut into 8 to 10 small pieces and dispersed in enzyme buffer (trypsin 0.3 mg/mL and DNAase 0.3 mg/mL in Ca^{2+}-free Krebs buffer). The cardi-
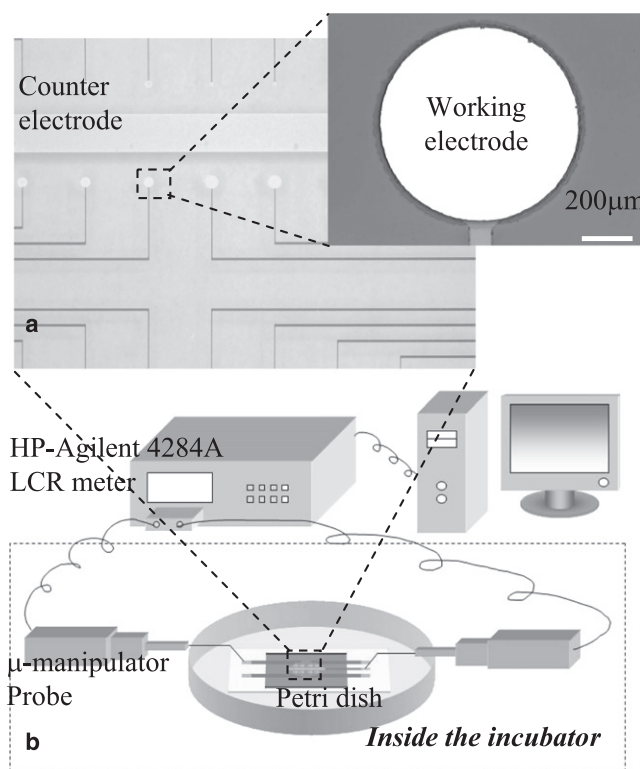

FIGURE 1 (a) Top view and close view of the counter and testing electrodes fabricated in a lift-off process (Cr/Au: 125 Å/375 Å). Chromium was used to increase the adhesion of the gold layer to the glass substrate. A laminin (an ECM protein) layer was coated before cardiomyocytes were injected. (b) Schematic diagram of the impedance measurement system. The part surrounded by dashed lines is inside the incubator (37°C, 5% CO_2).

omyocyte suspension was subsequently filtered through a nylon mesh, resulting in a typical yield of >90% rod-shaped cells. The isolated cells were then washed with Dulbecco's Modified Eagle Medium and were ready for plating onto microelectrodes. For the ECM, a laminin suspension was prepared by diluting the laminin solution (Becton-Dickinson, Franklin Lakes, NJ) in serum-free medium at volume ratio of 1:100. The laminin suspension was dropped onto the impedance-sensing electrodes, which were then kept still in the incubator for at least 30 min until a laminin layer formed. For electrical measurement, the biosensing chip was inoculated with 1.5 mL of the cardiomyocyte suspension, leading to a concentration of 5×10^4 cells/cm^2 of electrode area.

Frequency scanning and impedance spectroscopy

The measurement of impedance was performed with 80 frequencies logarithmically spaced between 20 Hz and 200 kHz with a 5-mV voltage excitation. One round of frequency scanning was completed in 1 min. For continuous monitoring, cyclic frequency scanning was applied to the testing system every 10 min. The impedance data were recorded as real and imaginary components accompanied by the testing frequency in a.txt file, which was convenient for the following data processing and analysis.

Despite the existing curve-fitting software, for example, LEVM, a complex nonlinear least-square (CNLS) curve fitting program was written based on the optimizing toolbox of MATLAB. This provided a convenient approach to process the impedance data obtained through the LabView virtual instrument and to carry out the following calculations and plotting.

TNF-α treatment and evaluation of cell viability and apoptosis

TNF-α (Sigma-Aldrich, St. Louis, MO) treatment was carried out in serum-free medium after 24-h culture for stabilization. Cardiomyocytes were incubated with different concentrations of TNF-α for 24 h. Cyclic frequency scanning was applied to the samples as soon as the TNF-α treatment began.

Evaluation of cell viability was conducted with TBE test in which 0.4% Trypan blue solution (Sigma-Aldrich) was used. The applied concentration of Trypan blue was 5% v/v. The samples were analyzed on a fluorescent microscope (Nikon Eclipse TS100-F; Nikon Instruments, Melville, N.Y.). More than 700 cells were counted in 10 fields for each independent experiment.

Apoptosis was detected with the TUNEL test in which the In Situ Cell Death Detection Kit, Fluorescein (Roche Applied Science, Indianapolis, IN) was used. After the treatment with TNF-α, cardiomyocytes were washed three times in phosphate-buffered saline (PBS) and then fixed with 4% para-formaldehyde in PBS for 1 h at room temperature. Cardiomyocytes were then permeabilized for 2 min on ice with 0.1% Triton X-100 in 0.1% sodium citrate. After two rinses with PBS, 50 μL TUNEL reaction mixtures were added on the cardiomyocytes, followed by incubation for 1 h in a humidified and dark chamber. Cardiomyocytes were rinsed three times with PBS and strained with 4',6-diamidino-2-phenylindole (DAPI). More than 500 cells were counted in 10 fields for each independent experiment.

RESULTS AND DISCUSSION

Characterization of the impedance-sensing system

In our experimental setup, cardiomyocytes were cultured on the electrode covered by ECM protein, specifically laminin. The impedance spectra were recorded before and after addition of freshly isolated cardiomyocytes into the suspension, so that the characteristics of the cell-free and cell-covered impedance-sensing system could be determined and described with equivalent circuit models.

Impedance analysis of the cell-free system

The impedance-sensing system without cells (Z_n) can be represented by the equivalent circuit model shown in Fig. 2 *a*. Here, the dielectric characteristics of the protein layer (laminin) are considered an ideal capacitor (C_p) on the electrode surface. However, because laminin consists of macromolecules of ~900 kDa in molecular mass and ~10 nm in length (21), it is difficult to achieve complete and compact coverage of laminin over the electrode surface. Research does demonstrate that pores exist among the macroprotein molecules (22). Solution can enter these poles and reach the gold electrode surface (Fig. 2 *b*), which can induce nonideal capacitance and resistance. Therefore, a constant-phase element (CPE) is used to account for the nonlinearities of frequency-related electrical double-layer impedance ($Z_{CPE} = [Q_{CPE}(j\omega)^n]^{-1}$, where j and ω are the imaginary unit and angular frequency, respectively) on the naked gold surface (23,24). The resistor R_p is used to represent the pore resistance in the laminin layer. Both the current flows via protein molecules and via pores in the protein coating layer travel in the bulk medium represented with a resistor (R_s').
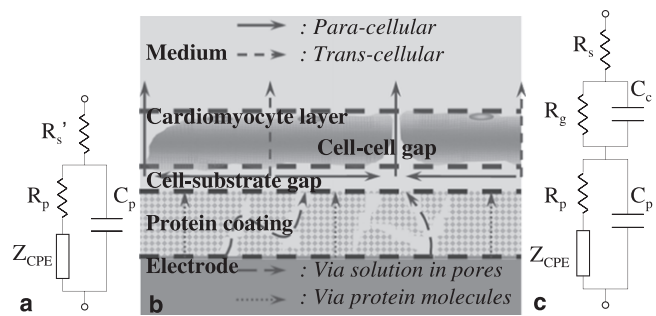

FIGURE 2 (*a*) Equivalent circuit model of system impedance without cells. R_s' is the resistance of bulk solution and the wire connection. The capacitance of the laminin layer is represented by C_p. Z_{CPE} and R_p are used to describe nonideal capacitive response of the uncovered electrode surface and the resistance in the pores of the laminin layer. (*b*) Current flow patterns on the testing electrode. There are two modes of current in the protein coating layer: one travels via solution in the pores among protein molecules; the other travels via protein molecules. There are also two modes of current in the cardiomyocyte layer: the paracellular mode represents how the current travels in solution around cells; the transcellular mode represents how the current travels through the cell body. (*c*) Equivalent circuit model of impedance of the cell-covered electrode (Z_c). The impedance response to paracellular or transcellular current is described with resistors or capacitors, respectively. Specifically, R_g is the resistance of the medium layer in the cell-substrate and cell-cell gap. When cardiomyocytes begin to adhere to ECM protein, the decrease in the cell-substrate gap will result in an increase in R_g.

The equivalent circuit model was fit to the three-dimensional impedance response plot of the impedance-sensing system, as shown in Fig. 3 *a*. To determine the element parameters of the impedance-sensing system, the CNLS curve fitting was performed to the equivalent circuit model in Fig. 2 *a*. The P weighting (25) was added into the objective function of CNLS curve fitting to ensure the validity in case the fitting to the real or imaginary component of impedance was unbalanced. The element parameters were determined for the cell-free impedance-sensing system: $R_s' = 2.22 \pm 0.03\ \Omega\ cm^2$, $C_p = 5.46 \pm 0.13\ \mu F/cm^2$, $R_p = 2.25 \pm 0.23\ \Omega\ cm^2$, $Q_{CPE} = 124.92 \pm 0.33\ \mu F/cm^2$, $n = 0.805 \pm 0.003$.

Impedance analysis of the cell-covered system

Once the cell-free system had been characterized, the medium containing laminin was drained and replaced with the cardiomyocyte suspension. After the cells settled down on the biosensing chip, the total impedance (Z_c) could be considered as the combination of cell-related impedance (Z_r) and Z_n with the exception of R_s' ($Z_r = Z_c - (Z_n - R_s')$). We built the cardiomyocyte layer model on an electrode based on EIS. In our equivalent circuit model of Z_r (Fig. 2 *c*), C_c is used to represent the reactance of cells, and R_g is used to describe the resistance of the thin medium layer in the cell-substrate and cell-cell gap. R_s is the resistance of bulk medium body. To achieve automation of the data processing, the admittance response ($Y_r = 1/Z_r$) in a Nyquist plot was first characterized (19). The electrical parameters acquired in the Nyquist plots
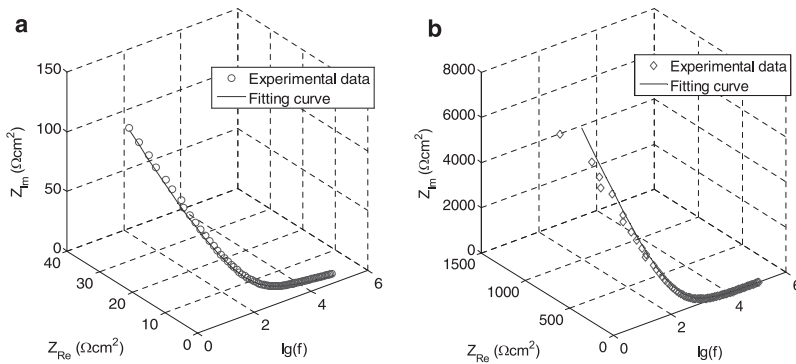
FIGURE 3 (*a*) Characterization of cell-free impedance sensing system (Z_n) with CNLS curve fitting with P weighting in the objective function. The curve fitting was performed with a program developed from the optimizing function toolbox of MATLAB. According to the convention of the electrochemical society, $Z = Z_{Re} - jZ_{Im}$. (*b*) CNLS curve fitting of the cell-related impedance to the EIS model with P weighting in the objective function. The related electrical parameters R_g, R_s, and C_c are determined.

of Y_r were utilized as the iterative initial points of the following CNLS curve fitting. As shown in Fig. 3 *b*, the best fit of cell-related impedance spectra was obtained with $R_g = 2.71 \pm 0.09\ \Omega\ m^2$, $C_c = 1.04 \pm 0.05\ \mu F/cm^2$, and $R_s = 2.39 \pm 0.16\ \Omega\ cm^2$. Every loop in the cyclic frequency scanning went through the EIS data processing to determine R_g, C_c, and R_s values.

Specifically, because the cell-substrate and cell-cell gaps change synchronously, the variation of R_g could be assumed inversely proportional to that of normalized cell-substrate distance because the R_g was present because of the resistivity of the conductive solution, which obeyed the Ohm's law (19). The automatic recording of R_g could be translated into a time course of normalized cell-substrate distance.

ECIS calibration of absolute cell-substrate distance

The calibration of absolute cell-substrate distance was performed with Lo's cell model (16) and the cell-related electrical parameter extracted above. Especially, the impedance through the body of the cell was considered as the capacitive reactance of cell membrane, which filled in the gap of unknown electrical properties of primary cardiomyocytes in ECIS calibration.

Lo's cell model (16) was described as a flat rectangular ($L \times W$) box and a half-disk ($r_c = W/2$) on each end. In this method, specific impedances of cell-covered (Z_c) and cell-free (Z_n) electrodes were calculated by multiplying the measured impedance by the electrode area. The impedance through a cell body was expressed as the reactance of C_c in the EIS model: $Z_m = -j/(\omega C_c)$. The best fit of ECIS (Fig. 4) was obtained with absolute cell-substrate distance of 59.1 ± 2.0 nm and junctional resistance among cells of $2.34 \pm 0.09\ \Omega\ m^2$.

Although the absolute cell-substrate distance could be obtained through ECIS calibration, the absence of iterative initial points restricted its application in processing isolated data at a single moment. To achieve the continuous recording of cell adhesion, the time course of equivalent cell-substrate distance was defined as the product of the time course of normalized cell-substrate distance and absolute value obtained in ECIS calibration.

Real-time monitoring of cardiomyocyte death

The cell-substrate distance would be an ideal parameter to quantify the extent of cell adhesion, which was highly related to cell responses to various stimuli. Freshly isolated cardiomyocytes were first cultured on the working electrodes for 24 h to achieve a stable adhesion to ECM. The equivalent cell-substrate distance was then recorded for the cardiomyocytes that were undergoing cell death. TBE and TUNEL assays were employed to prove the occurrence of cell death and apoptosis, respectively.

Concentration-related adhesion profiles of cardiomyocyte death

Cardiomyocytes treated with different concentrations of TNF-α exhibited distinct adhesion profiles, i.e., the increasing rate and extent of equivalent cell-substrate distance. Fig. 5 *a* showed the representative results of three independent experiments in which five concentrations of TNF-α were applied (0 to ~80 ng/mL). Although the initial
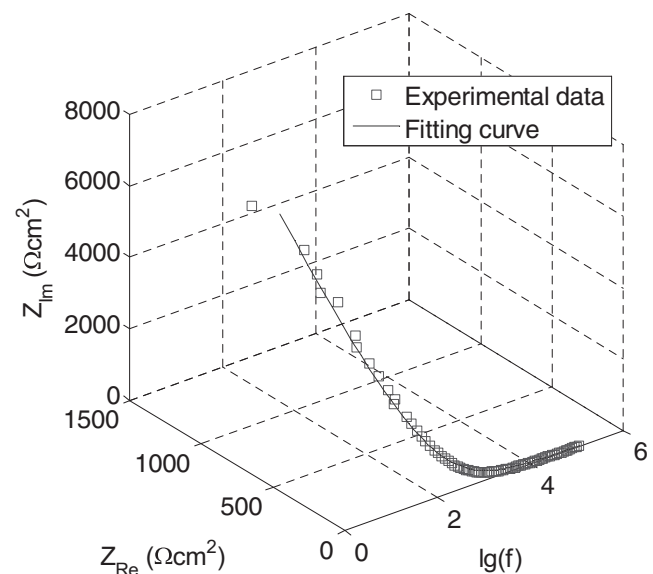

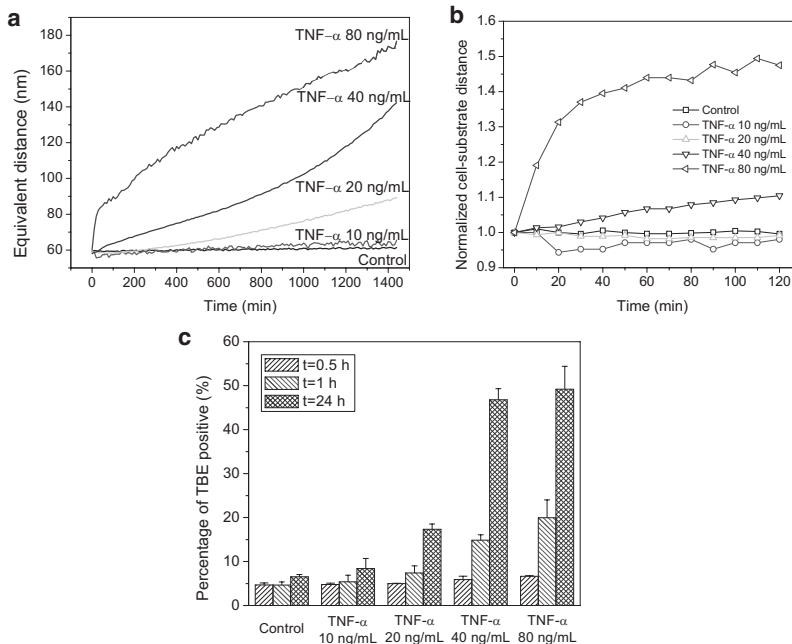FIGURE 4 ECIS calibration of absolute cell-substrate distance based on Lo's cell model (16).

FIGURE 5 (a) Adhesion profiles of cardiomyocytes treated continuously with different concentrations of TNF-α. (b) Adhesion profiles of treated cardiomyocytes in the first 2 h. For comparison, equivalent cell-substrate distances were normalized to their respective initial values. (c) Percentage of death obtained with TBE tests in treated cardiomyocytes at $t = 0.5$ h, $t = 1$ h, and $t = 24$ h. Data from three independent experiments are shown as mean ± SD.

equivalent distances were close, the five curves were distinct from each other in the 24-h continuous recording. At the end of treatment, the final distances varied from 61.3 nm to 176.7 nm, which were in an increasing order of TNF-α concentration. The increase of cell-substrate distance was a result of ongoing cell death, including apoptosis and necrosis, in which cell detachment would occur no matter which death mechanism was dominant. The diversity in increasing amplitude could be caused by the different percentages of cardiomyocytes ongoing cell death. It indicated the concentration of TNF-α was an important experimental factor in inducing cell death of cardiomyocytes. Furthermore, the increasing rates of equivalent cell-substrate distance were also strongly influenced by the TNF-α concentration. The samples treated with higher concentrations exhibited faster ascent than those with lower concentrations. Especially at the beginning stage of treatment, the 10 and 20 ng/mL samples experienced a drop in equivalent distance for ~2 h and then continued ascent at slow rates in the following hours. On the contrary, the 40 and 80 ng/mL samples began to detach from the ECM immediately after addition of TNF-α (Fig. 5 b). The increasing rate of equivalent distance was determined by the rate of cell death percentage. Because the apoptotic process was much slower than the necrotic process as a result of differences between two mechanisms, necrosis could be predominant in the fast rate of cell death percentage that was observed in the cardiomyocytes treated with higher concentrations of TNF-α.

The cell detachment observed in our assay was related to the activation of the TNF-α-induced cardiomyocyte death process. The TBE test was employed for the demonstration of cell death. Before the TNF-α treatment, the death percentage of cardiomyocytes was 3.3 ± 0.7%. After

30 min of treatment, even though no obvious difference could be found in the TBE results (Fig. 5 c), cell detachment was observed with our assay in the 40 and 80 ng/mL TNF-α-treated samples. The rapid cell detachment was related to the cell death in the following TBE tests at $t = 1$ h in which the death percentages of samples treated with 40 and 80 ng/mL TNF-α were remarkably higher than those of other samples. The early detection of cell detachment provided us real-time information about ongoing cell death in cardiomyocytes before the TBE tests. Furthermore, because it takes at least 2 h to activate the caspase family for the execution of TNF-α-induced apoptosis (26), the TBE-positive cardiomyocytes observed at $t = 1$ h were undergoing necrosis rather than apoptosis. On the other hand, samples treated with 10 and 20 ng/mL did not exhibit an obviously higher percentage of TBE-positive than the control, indicating that the chemical stimuli induced very mild necrosis, even no necrosis, in these samples. After 24-h TNF-α treatment, the death percentage of cells obviously increased and expressed a monotonically increasing relation with the TNF-α concentration. The control and 10 ng/mL samples showed only very little increment in cell death; meanwhile the death percentages of samples at the concentration of 20 ng/mL and above significantly increased from their amounts at $t = 1$ h. These profiles of death percentage were similar to those of cell-substrate distance, indicating the coherence of these two methods.

Apoptosis-dominant cardiomyocyte death

Because the cardiomyocyte sample treated with 20 ng/mL TNF-α exhibited no obvious cell death at both $t = 0.5$ h and $t = 1$ h but significant death percentage at $t = 24$ h
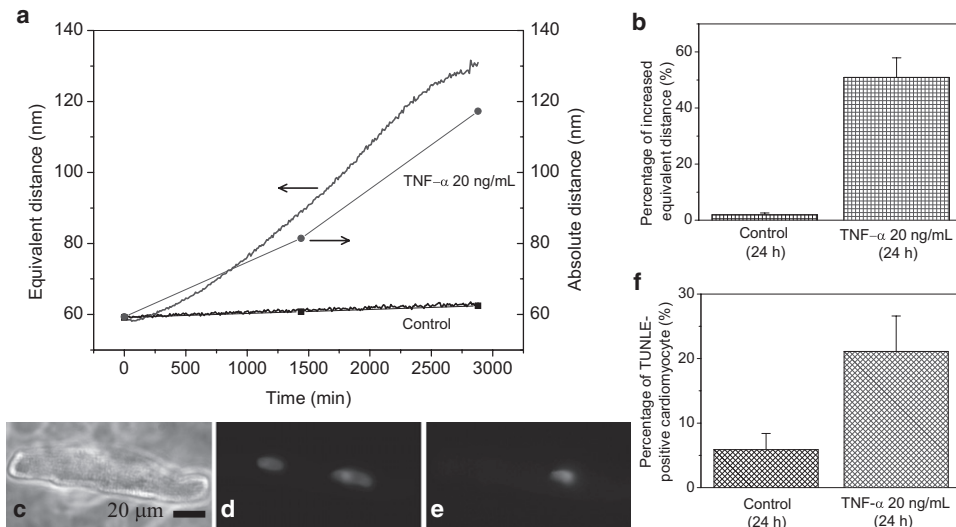
FIGURE 6 (*a*) Real-time recording of cardiomyocyte adhesion in terms of equivalent cell-substrate distance (*solid line*) and absolute cell-substrate distance (*scattered dots with line*). The treatment was carried out on the cardiomyocytes with 20 ng/mL TNF-α. (*b*) Percentages of increase in equivalent distance of TNF-α-treated and control samples at $t = 24$ h. (*c*) Phase-contrast image of the TNF-α-treated sample. (*d*) Corresponding fluorescent image of the DAPI-stained TNF-α-treated sample. (*e*) Corresponding fluorescent image of the TUNEL-stained TNF-α-treated sample. (*f*) Percentage of TUNEL-positive cardiomyocytes TNF-α-treated and control samples at $t = 24$ h ($p < 0.01$).

(Fig. 5 *c*), it was possible that apoptosis was at least involved. According to published reports (27–30), TNF-α induces caspase-involved apoptotic signaling pathways in cardiomyocytes as an extracellular messenger protein. The activation of the caspase family will cause the detachment of cardiomyocytes from the ECM or neighbor cells by cleaving some essential proteins including focal adhesion kinase. Because the activation of the caspase family occurs soon after the binding of TNF-α to TNF receptors, the cell detachment is expected to be seen not long after the treatment. The 2-day recording of cell-substrate distance was plotted in Fig. 6 *a*, where the solid lines were the alteration of equivalent cell-substrate distance. The addition of TNF-α induced a rapid increase in equivalent cell-substrate distance after a lag phase of ~2 h, which might be caused by the time needed to activate the caspase family (26). The increasing rate of equivalent distance slowly speeded up in the first day and gently slowed down in ~2 days. The total increasing amplitude of the treated sample was 61.8 nm, whereas that of the control sample was 3.2 nm. We also compared the equivalent cell-substrate distance with the absolute distance calculated via advanced ECIS. Besides the initial absolute distance, the values at $t = 24$ h and $t = 48$ h were also plotted in Fig. 6 *a* as scattered dots. The results showed the good coherence of equivalent and absolute cell-substrate distance. In short, TNF-α induced a significant increase in equivalent cell-substrate distance (Fig. 6 *b*), which was caused by weakening cell adhesion to ECM of the treated cardiomyocytes.

To determine whether apoptosis occurred to the cardiomyocytes treated with 20 ng/mL TNF-α, the TUNEL tests were carried out for the calibration of apoptosis. Fig. 6, *c–e*, showed the corresponding phase contrast, DAPI-staining fluorescent, and TUNEL-staining fluorescent images of a TNF-α-treated cardiomyocytes (at $t = 24$ h) in which DNA fragmentation was indicated. The results of three independent experiments were plotted in Fig. 6 *f*. After 24-h

treatment with 20 ng/mL TNF-α, cardiomyocytes with TUNEL positive were significantly increased (i.e., $21.1 \pm 5.5\%$ versus $5.9 \pm 2.5\%$ in time control, $p < 0.01$), indicating that the degree of cardiomyocyte apoptosis was prompted by TNF-α treatment. As shown in the TBE tests, the death percentage was $17.3 \pm 1.2\%$ at the same moment. The apoptotic percentage was close to the total death percentage, indicating that apoptosis was the major death mechanism in the 20 ng/mL sample. The cell detachment monitored in our assay reflected the dynamic process of apoptotic cell death, which was presented in a unique adhesion profile. Generally speaking, the adhesion profile gathered with our methodology is a very direct and visual indicator of cell morphology, which can enrich the technical approaches to reveal cell responses.

CONCLUSION

In this work, a new impedance-based bioelectric assay was developed for real-time monitoring of ongoing cardiomyocyte death induced by TNF-α. The profile of cardiomyocyte adhesion to ECM in terms of equivalent cell-substrate distance could be obtained via the combination of EIS and electric cell-substrate impedance sensing. The dynamic process of cell detachment obtained with our assay was proved to be related to cell death, which suggested the possibility of predicting the consequent bioprocess. It was also demonstrated that our assay could also achieve early detection of cell death earlier than Trypan blue tests. This novel assay has the potential to become a valuable high-throughput experimental approach to the research of cardiomyocytes.

REFERENCES

1. Nakayama, H., X. Chen, C. P. Baines, R. Klevitsky, X. Zhang, et al. 2007. Ca^{2+}- and mitochondrial-dependent cardiomyocyte necrosis as a primary mediator of heart failure. *J. Clin. Invest.* 117:2431–2444.

2. Giaever, I., and C. R. Keese. 1984. Monitoring fibroblast behavior in tissue culture with an applied electric field. *Proc. Natl. Acad. Sci. USA.* 81:3761–3764.

3. Giaever, I., and C. R. Keese. 1993. A morphological biosensor for mammalian cells. *Nature.* 366:591–592.

4. Xiao, C. D., B. Lachance, G. Sunahara, and J. H. T. Luong. 2002. Assessment of cytotoxicity using electric cell-substrate impedance sensing: Concentration and time response function approach. *Anal. Chem.* 74:5748–5753.

5. Luong, J. H. T., M. Habibi-Rezaei, J. Meghrous, C. Xiao, K. B. Male, et al. 2001. Monitoring motility, spreading, and mortality of adherent insect cells using an impedance sensor. *Anal. Chem.* 73:1844–1848.

6. Xiao, C., B. Lachance, G. Sunahara, and J. H. Luong. 2002. An in-depth analysis of electric cell-substrate impedance sensing to study the attachment and spreading of mammalian cells. *Anal. Chem.* 74:1333–1339.

7. Kowolenko, M., C. R. Keese, D. A. Lawrence, and I. Giaever. 1990. Measurement of macrophage adherence and spreading with weak electric fields. *J. Immunol. Methods.* 127:71–77.

8. Mitra, P., C. R. Keese, and I. Giaever. 1991. Electric measurements can be used to monitor the attachment and spreading of cells in tissue culture. *Biotechniques.* 11:504–510.

9. Tiruppathi, C., A. B. Malik, P. J. Del Vecchio, C. R. Keese, and I. Giaever. 1992. Electrical method for detection of endothelial cell shape change in real time: assessment of endothelial barrier function. *Proc. Natl. Acad. Sci. USA.* 89:7919–7923.

10. Sapper, A., J. Wegener, and A. Janshoff. 2006. Cell motility probed by noise analysis of thickness shear mode resonators. *Anal. Chem.* 78:5184–5191.

11. Earley, S., and G. E. Plopper. 2006. Disruption of focal adhesion kinase slows transendothelial migration of AU-565 breast cancer cells. *Biochem. Biophys. Res. Commun.* 350:405–412.

12. Aas, V., S. Torbla, M. H. Andersen, J. Jensen, and A. C. Rustan. 2002. Electrical stimulation improves insulin responses in a human skeletal muscle cell model of hyperglycemia. *Ann. N.Y. Acad. Sci.* 967:506–515.

13. Yang, M., C. C. Lim, R. Liao, and X. Zhang. 2007. A novel microfluidic impedance assay for monitoring endothelin-induced cardiomyocyte hypertrophy. *Biosens. Bioelectron.* 22:1688–1693.

14. Yang, M., and X. Zhang. 2007. A novel impedance assay for cardiac myocyte hypertrophy sensing. *Sens. Actuators A Phys.* 136:504–509.

15. Giaever, I., and C. R. Keese. 1991. Micromotion of mammalian cells measured electrically. *Proc. Natl. Acad. Sci. USA.* 88:7896–7900.

16. Lo, C. M., and J. Ferrier. 1998. Impedance analysis of fibroblastic cell layers measured by electric cell-substrate impedance sensing. *Phys. Rev. E Stat. Phys. Plasmas Fluids Relat. Interdiscip. Topics.* 57:6982–6987.

17. Lo, C. M., C. R. Keese, and I. Giaever. 1995. Impedance analysis of MDCK cells measured by electric cell-substrate impedance sensing. *Biophys. J.* 69:2800–2807.

18. Arndt, S., J. Seebach, K. Psathaki, H. J. Galla, and J. Wegener. 2004. Bioelectrical impedance assay to monitor changes in cell shape during apoptosis. *Biosens. Bioelectron.* 19:583–594.

19. Qiu, Y., R. Liao, and X. Zhang. 2008. Real-time monitoring primary cardiomyocyte adhesion based on electrochemical impedance spectroscopy and electrical cell-substrate impedance sensing. *Anal. Chem.* 80:990–996.

20. Lim, C. C., M. H. Helmes, D. B. Sawyer, M. Jain, and R. Liao. 2001. High-throughput assessment of calcium sensitivity in skinned cardiac myocytes. *Am. J. Physiol. Heart Circ. Physiol.* 281:H969–H974.

21. Beck, K., I. Hunter, and J. Engel. 1990. Structure and function of laminin: anatomy of a multidomain glycoprotein. *FASEB J.* 4:148–160.

22. Freire, E., F. C. Gomes, R. Linden, V. M. Neto, and T. Coelho-Sampaio. 2002. Structure of laminin substrate modulates cellular signaling for neuritogenesis. *J. Cell Sci.* 115:4867–4876.

23. Bard, A. J., and L. R. Faulkner. 2003. Electrochemical Methods: Fundamentals and Applications. John Wiley & Sons, Hoboken, NJ.

24. Tlili, C., K. Reybier, A. Geloen, L. Ponsonnet, C. Martelet, et al. 2003. Fibroblast cells: a sensing bioelement for glucose detection by impedance spectroscopy. *Anal. Chem.* 75:3340–3344.

25. Barsoukov, E., and J. R. Macdonald. 2005. Impedance Spectroscopy. John Wiley & Sons, Hoboken, NJ.

26. Bajaj, G., and R. K. Sharma. 2006. TNF-alpha-mediated cardiomyocyte apoptosis involves caspase-12 and calpain. *Biochem. Biophys. Res. Commun.* 345:1558–1564.

27. Zhu, J., M. Liu, R. H. Kennedy, and S. J. Liu. 2006. TNF-alpha-induced impairment of mitochondrial integrity and apoptosis mediated by caspase-8 in adult ventricular myocytes. *Cytokine.* 34:96–105.

28. Krown, K. A., M. T. Page, C. Nguyen, D. Zechner, V. Gutierrez, et al. 1996. Tumor necrosis factor alpha-induced apoptosis in cardiac myocytes. Involvement of the sphingolipid signaling cascade in cardiac cell death. *J. Clin. Invest.* 98:2854–2865.

29. Song, W., X. Lu, and Q. Feng. 2000. Tumor necrosis factor-alpha induces apoptosis via inducible nitric oxide synthase in neonatal mouse cardiomyocytes. *Cardiovasc. Res.* 45:595–602.

30. Takahashi, R., Y. Sonoda, D. Ichikawa, N. Yoshida, A. Y. Eriko, and K. Tadashi. 2007. Focal adhesion kinase determines the fate of death or survival of cells in response to TNFalpha in the presence of actinomycin D. *Biochim. Biophys. Acta.* 1770:518–526.